Solar Energy Materials & Solar Cells 153 (2016) 164–178

Contents lists available at ScienceDirect

Solar Energy Materials & Solar Cells

journal homepage: www.elsevier.com/locate/solmat

Performance, limits and economic perspectives for passive cooling of High Concentrator Photovoltaics

Leonardo Micheli [a,*], Eduardo F. Fernández [b,c], Florencia Almonacid [b,c], Tapas K. Mallick [a], Greg P. Smestad [d]

[a] Environment and Sustainability Institute, University of Exeter, Penryn Campus, Penryn TR10 9FE, UK
[b] Centre for Advanced Studies in Energy and Environment, University of Jaen, Las Lagunillas Campus, Jaen 23071, Spain
[c] IDEA Solar Energy Research Group, University of Jaen, Las Lagunillas Campus, Jaen 23071, Spain
[d] Sol Ideas Technology Development, San José, CA 95150, USA

ARTICLE INFO

Article history:
Received 26 November 2015
Received in revised form
25 February 2016
Accepted 10 April 2016

Keywords:
Thermal materials
High Concentrator Photovoltaics
Cell temperature
Passive cooling
Electrical performance
Energy economics

ABSTRACT

This paper provides an analysis of the benefits of passive cooling for High Concentrator Photovoltaic (HCPV) systems in terms of costs and kWh annual energy yields. For the first time, the performance of the heat sinks has been related to the calculated energy yield of a standard triple-junction GaInP/GaAs/Ge HCPV cell in a system deployed at several suitable locations across the globe. Copper and aluminium heat sinks have been considered and their merits have been compared. The finite element analysis software package COMSOL was employed to gain insights regarding a simple flat plate heat sink. The cell temperature was found to have a linear dependence on the geometric concentration with a characteristic slope that increases with cell size (ranging from 10 to 0.25 mm). The results show the advantages of miniaturisation, and that the cooling of smaller cells can be accomplished using flat heat sinks. Within the considered range of geometric concentration ratios (up to 1000 ×), aluminium heat sinks are, in general, found to be preferred over copper, because of their lower densities and costs for the same thermal management. Closed-form thermal models based on the Least-Material (LM) approach have been utilised to design more complex finned heat sinks (operated under natural convection) that yield the best compromise between thermal performance and weight. For a 60 °C cell operating temperature, a greater kWh output is obtained, but an LM heat sink designed for a cell temperature of 80 °C has a material cost per unit energy that is between 50% and 70% less than the one designed for 60 °C. Heat sink costs between $0.1 and 0.9 per W_p were estimated for a geometric concentration above 500 suns, depending on the cell's temperature and size. There are strong reductions in HCPV installation costs by limiting the dimensions of the cooling system at high concentrations.

1. Introduction

High Concentrator Photovoltaic (HCPV) systems use lenses or mirrors to concentrate sunlight by more than three hundred times on a solar cell [1,2]. For HCPV systems, the employment of high-efficiency multijunction (MJ) cells becomes more convenient than using large area traditional silicon cells [3]. Impressive progress has been recently reported with regard to MJ cells, which have achieved record-efficiencies up to 46% [4]. Despite this development, the largest part of the incoming solar energy is still converted into heat, which can lead to an increase in cell temperature [5,6]. Any photovoltaic cell is negatively affected by the increase of temperature and this becomes a non-negligible concern in HCPV systems, due to the high current densities and heat fluxes experienced [7]. Therefore, HCPV systems are generally coupled to a cooling system, able to remove the heat generated by the cell and to transfer it to an external medium. In order to keep the HCPV cells at temperatures ranging between 50 °C and 80 °C [8,9], different cooling systems have been proposed and explored experimentally in the past [10–13]. The present work focuses on passive cooling systems, as those solutions do not require any electrical or mechanical energy input to operate. Passive cooling technologies have been proved able to successfully handle the thermal management of single cell HCPV modules at high and ultra-high concentrations [13–17], thanks to the large surface available for heat transfer.

HCPV modules are typically placed on trackers. Since they use only the direct component of the sunlight, they have to follow the

* Corresponding author. Tel.: +44 0 1326259478.
E-mail addresses: l.micheli@exeter.ac.uk (L. Micheli), fenandez@ujaen.es (E.F. Fernández), facruz@ujaen.es (F. Almonacid), t.k.mallick@exeter.ac.uk (T.K. Mallick), inquiries@solideas.com (G.P. Smestad).

http://dx.doi.org/10.1016/j.solmat.2016.04.016

Nomenclature

Symbol	Definition units
A	area ($m^{2)}$
C_{geo}	geometric concentration (×)
C_m	cost per unit of mass (USD/kg)
c_{macHS}	cost of machined heat sink (USD)
DNI	Direct Normal Irradiance ($W/m^{2)}$
E	annual energy yield (kWh)
E_b	incident direct normal spectral distribution (W/m^2 nm)
$E_{b,\ ref}$	direct reference spectrum (W/m^2 nm)
$F_{i,j}$	view factors between the surfaces i and k ($0 \le F_{i,j} \le 1$) (dimensionless)
g	gravitational acceleration ($m/s^{2)}$
H	fin height (m)
h_c	heat transfer coefficient (W/m^2 K)
k	thermal conductivity (W/m K)
L	fin length (m)
l	distance between the heat source and the heat sink (m)
L^*	characteristic length (m)
LCOE	levelised cost of the electricity ($/kWh)
MBE	mean bias error (%)
N	useful life of the system years
n_{fin}	number of fins (dimensionless)
p	pitch of the fin array (m)
P	electrical power output (W)
Pr	Prandtl number (dimensionless)
Q	heat power (W)
R	thermal resistance (K/W)
Ra_L	Rayleigh number (dimensionless)
RMSE	root mean square error (%)
s	spacing between fins (m)
SF	spectral factor (dimensionless)
SR	spectral response (A/W)
t	fin thickness (m)
T	temperature (K)
T^*	nominal temperature (K)
t_b	fin base thickness (m)
TF	thermal factor (dimensionless)
W	fin base width (m)

Greek letters

α	thermal diffusivity (m^2/s)
β	thermal expansion coefficient of air (1/K)
γ	power temperature coefficient (%/K)
ε	emissivity ($0 \le \varepsilon \le 1$) (dimensionless)
η_{cell}	cell electrical efficiency ($0 \le \eta_{cell} \le 1$) (dimensionless)
η_{fin}	fin efficiency ($0 \le \eta_{fin} \le 1$) (dimensionless)
η_{opt}	optical efficiency ($0 \le \eta_{opt} \le 1$) (dimensionless)
θ_b	difference of temperature between the heat sink and the ambient (K)
ν	mean kinematic viscosity of air (m^2/s)
ρ	density ($kg/m^{3)}$
σ	Stefan–Boltzmann constant (W/m^2 $K^{4)}$

Subscripts

amb	ambient
c	convection
cell	cell
HS	heat sink
k	conduction
opt	optimal value according to the LM approach
surr	surrounding fluid

Abbreviations

AM	Air Mass
DBC	Direct Bonded Copper
HCPV	High Concentrator Photovoltaics
LM	Least-Material (approach)
MJ	Multi-Junction (cells)

Sun's apparent motion in order to keep the direct component of sunlight focused on the cells [18]. This said, limiting the weight of the tracked components becomes particularly important in order to reduce the load on the tracker and thus its energy consumption and its volume. Along with the intrinsic weight of the system, the tracker is required to withstand wind forces, whose torque effect increases with the weight of the solar modules and the supporting structure [19]. Misalignments between the optics and the cells, caused by the actions of wind on the trackers, can strongly affect the energy production [20]. So, in addition to the lower energy consumption, a reduced weight of the module would allow reducing the cost of fabrication of the tracker, since less material would be required to support lighter structures. Heat sinks are generally made of aluminium, which can represent more than 60% of the weight of an HCPV system [21]. Therefore, the best compromise between the weight and the performance of the heat sink has to be realized in order to limit the load on the tracker and, at the same time, to enhance the electrical output of the HCPV system. Moreover, the contribution of the heat sink to the cost of the energy cannot be neglected [22]. Recent studies [23,24] concluded that HCPV can already be more profitable than standard flat PV in high Direct Normal Irradiance (DNI) regions. Additional reductions in cost have to be achieved in order to further improve the cost competitiveness of HCPV. Optimised, light-weight passive heat sinks can positively affect the cost of HCPV by reducing the volumes of the materials, minimising the energy consumption of the tracker and enhancing the electrical performance of the cells.

One of the most common passive cooling solutions in HCPV is the use of a metal plate heat sink. Araki et al. [15] first demonstrated the possibility of cooling a 500x cell by using an aluminium plate. Min et al. [25] proposed a model to predict the behaviour of a single 3 mm × 3 mm cell by taking into account a fixed heat transfer coefficient of 5 W/m^2. Renzi et al. [26] studied the outdoor performance of a 5.5 mm × 5.5 mm cell under a geometric concentration of 476 × . The authors found that the aluminium plate reached a temperature between 55 °C and 65 °C, but no information on the cell temperature was given. Gualdi et al. [27] showed that flat plates can keep cells with dimensions smaller than 4 mm below a temperature of 80 °C. The use of fins is considered the easiest way to enhance the heat transfer between a surface and a surrounding fluid [28]. Fins are widely used in several fields where cooling is required [29], from electronics to industrial applications. The use of fins has been investigated for CPV applications [30–32]. Natarajan and his collaborators [30] showed that fins are a more effective way to reduce the solar cell temperature than a flat back plate and identified the optimum fin dimensions for a 10 × CPV system. Do et al. [31] experimentally investigated the behaviour of passive finned heat sinks for different tilt angles. The authors

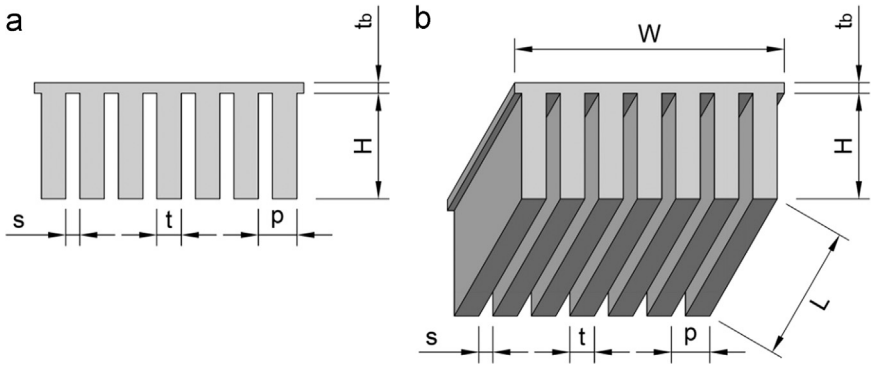

Fig. 1. Schematic of a finned heat sink: (a) front view and (b) 3D rendering. The nomenclature used in the present work is: spacing (s), pitch (p), height (H), thickness (t), length (L), base width (W), base thickness (t_b).

proposed a methodology to determine the heat transfer coefficient of a natural convective heat sink depending on the inclination angle and the fin spacing. Micheli et al. [32] demonstrated that micro-finned arrays could find an application for passive cooling of HCPV systems and commented on the benefits in terms of thermal performance and material usage that could be achieved. None of the previous works has investigated the thermal management of HCPV for different cell sizes and concentrations. The aim of the present paper is to provide an analysis of the benefits of passive cooling in HCPV in terms of costs and energy yields. The potentials and the limits of natural convective finned heat sinks are investigated and discussed. Different heat sink materials have been considered and their performance and weights have been compared and discussed. The present work has taken into account different cell sizes in order to analyse the effect of the miniaturization of the cells on the HCPV heat waste management. For the first time, the performance of the heat sinks has been related to the energy yield of an HCPV cell to give to system designers a useful metric for the development of future systems.

2. Materials and methods

2.1. Geometry of the heat sinks

In this work, a compact HCPV module has been considered, where the optics focus the sunlight on a single multijunction cell. An HCPV module is generally made of the optics, the cells, the bypass diode, the current extraction mechanisms and the natural convective finned heat sink [33]. The module is then usually mounted on a tracking system that keep the concentrated sunlight focused on the cell and the cell perpendicular to the beam in order to maximise the electrical performance. The straight fin geometry, represented in Fig. 1, has been considered in this work, because of its simple manufacturing and the large knowledge base available. The heat sinks investigated here have been designed using the Least-Material (LM) approach [34], a procedure to develop thermally optimized and low-volume heat sinks. Air is the cheapest, most available and common cooling fluid for HCPV systems [7] and has therefore been considered in the present investigation.

2.2. Heat sink design and modelling methods

Bar-Cohen et al. [34] proposed the LM approach, a model to design natural convective heat sinks with the best compromise between thermal performance and weight. The optimal spacing (s_{opt}) between the fins of an LM heat sink is expressed as [34]:

$$s_{opt} = 2.66 \cdot \left(\frac{L \cdot \nu^2}{g \cdot \beta \cdot \eta_{fin} \cdot \theta_b \cdot Pr} \right)^{0.25} \quad (1)$$

where ν is the mean kinematic viscosity of air, g is the gravitational acceleration, β is the thermal expansion coefficient of air, η_{fin} is the fin efficiency, θ_b is the difference of temperature between the heat sink and the ambient, and Pr is the Prandtl number. In this analysis, all the coefficients have been calculated at the average temperature between the fins and the ambient values, with the exception of the air's thermal expansion which was evaluated at ambient temperature [35]. As described in the paper presented by Bar-Cohen et al. [34] for the LM approach, the fin efficiency has to be set as 0.626 and the fin thickness (t_{opt}) is equal to the optimal fin spacing. The fin efficiency expresses the ratio of the heat effectively transferred by the fin to the maximum heat that would be transferred if the fin surface was at the temperature of the base [28]. The number of fins (n_{fin}) is then given by:

$$n_{fin} = \lceil \frac{W}{s_{opt} + t_{opt}} \rceil \quad (2)$$

Because the number of fins needs to be an integer, the value obtained is rounded up. For this reason, the value of the fin thickness is adjusted to make the fins fit on the base:

$$t^*_{opt} = \frac{W}{n_{fin}} - s_{opt} \quad (3)$$

The correlations reported by Bar-Cohen et al. [34] are valid for vertically orientated heat sinks, which facilitate the natural convective heat transfer between the fins and the ambient temperature. On the other hand, the downward orientation is the least effective orientation for heat sinks operating under natural convection conditions [36]. Despite that, in some cases, a downward facing orientation might be required due to the HCPV system's design. This is the case for HCPV, where, in some configurations [7], the heat sink is likely to be facing downward during the central hours of the day when the irradiance, and thus the waste heat produced by the cell, as well as the ambient temperature are at maximum. In order to predict the thermal performance of horizontal heat sinks, the LM approach has been integrated with the equations presented by Do et al. [31], where the experimental correlations between the orientation and the heat transfer coefficient of tilted heat sinks have been presented.

As shown by Bar-Cohen and his colleagues [34], the optimal fin height generally falls in an impractical range of values, out of the manufacturing technology possibility. Extruded fins generally achieve spacing ratios lower than 10 [37]. The spacing ratios have been limited in the present work as well. In particular, the optimal fin height (H_{opt}) has been designed to fall within the limits imposed

by Do et al. [31], in order to be able to use their model for the present analysis. Their validated experimental correlations give:

$$H_{opt} = 9 \cdot s_{opt} \quad (4)$$

In the present conservative approach, the heat sink is designed to operate even for the condition of no wind. That makes the transfer of heat more challenging: wind has a positive cooling effect on the CPV modules [20]. The LM approach [34] takes into account the convective heat transfer only. In real world applications, instead, it has been demonstrated that the effects of radiation should not be neglected, as it generally accounts for more than the 20% of the heat dissipated under natural convection conditions [38]. For this reason, the contribution of the radiative heat exchange from the fins has been introduced into the model using the Stefan–Boltzmann equation [28]:

$$Q_r = \sum_i \varepsilon \cdot \sigma \cdot A_i \cdot F_{i,j} \cdot \left(T_{fins}^4 - T_{surr}^4\right) \quad (5)$$

where ε is the emissivity of the heat sink material, σ is the Stefan–Boltzmann constant ($5.67 \cdot 10^{-8}$ W/m^2 K^4), A_i is the area of the correspondent *i*-surface of the fins, $F_{i,j}$ are the view factors between the surfaces i and j and T_{surr} is the temperature of the surrounding fluid. In accordance with previous literature [38], the surrounding medium is considered to be a large black body: so that, $T_{surr}=T_{amb}$. The view factors have been calculated according to the procedure suggested by Kulkarni and Das [39] and using the equations reported elsewhere [35].

The thermal models used in this work are already present in literature [31,34]. In order to prove their applicability in an HCPV environment, the results of the present investigation have been compared with the data available in literature for validation purposes. In addition, the multiphysics software package COMSOL 4.4 has been used for the thermal analysis. It exploits well-known heat transfer coefficient correlations defined in the literature [28]. Horizontal orientation in the absence of wind has been used as the geometric and ambient conditions in the model. In order to validate the assumptions made to conduct the present investigation, the setup used by Wang et al. [40], where a 23% efficient 476 × single cell module was investigated experimentally in zero wind conditions, has been modelled. Out of a measured reference temperature of 49 °C, the model developed for the present investigation predicted a cell temperature of 52 °C.

2.3. Materials and fabrication processes for HCPV heat sinks

Two different materials have been considered for the fabrication of the heat sinks [10]:

- Aluminium alloy EN AW-1050A [41], $k=229$ W/m K, $\rho=2700$ kg/m^3, cost of 1.587 USD per kg;
- Copper [42], $k=400$ W/m K, $\rho=8700$ kg/m^3, cost of 4.628 USD per kg;

where k is the thermal conductivity and ρ the density. The costs per unit mass of aluminium and copper reported in December 2015 by the London Metal Exchange have been used in the analysis [43]. The non-negligible contribution of radiation for a natural convective heat sink has already been demonstrated [38]. Therefore, heat sink manufacturers usually use (or apply) high-emissivity finishings or coatings in order to improve the contribution of radiative transfer in a natural convection environment. In this study, a high-emissivity finish has been taken into account for both materials in order to be able to present a consistent comparison between them. An anodised surface has been considered for aluminium, giving it an emissivity of $\varepsilon=0.84$ [41]. The copper surface can be covered by a black oxide layer able to increase the emissivity up to $\varepsilon=0.78$ [44]. Depending on the application, different finishes and coatings can be applied, varying the overall contribution of radiation.

The most common heat sink fabrication techniques are listed in Table 1. They are generally chosen on the basis of the application and are generally classified according to:

- The spacing ratio [34], which express the ratio of the fin height to the fin spacing (H/s).
- The cost, which includes the capital investment and the production expenses. It may differ depending on the production volume: high capital investment techniques, such as die-casting, become beneficial only for large-volume productions.

The main properties of each process are listed in Table 2. Additional manufacturing method characteristics can be taken into account, such as the fin geometry limitations, which vary among the different techniques. Extruded fin heat sinks are the most commonly employed and, for the scope of the present research, are considered in this work. In some circumstances, machined heat sinks have been taken into account as well. So, a comparison between the cost of Al and Cu heat sinks and an analysis of the wasted material could then be carried out.

A common geometry of an HCPV receiver is shown in Fig. 2, the typical materials and their properties are listed in Table 3. Standard triple-junction GaInP/GaAs/Ge cells have been considered. It is generally accepted to model the cell as a single block of germanium [17,48]. The top and middle subcells are much thinner than the bottom and therefore it has already been demonstrated that they would not affect the thermal model [49]. The cell is considered to have a fixed efficiency (η_{cell}) of 40% and different sizes have been taken into account: 10 mm × 10 mm, 3 mm × 3 mm and 0.25 mm × 0.25 mm. When not specified, the 3 mm × 3 mm cell has been considered, since it is among the smallest cells commercially available nowadays. Each cell is mounted on a Direct Bonded Copper (DBC) substrate through a lead-free SnAgCu solder. The DBC is then bonded to the substrate using a standard thermal interface material. The thicknesses of the receiver layers, specified in Table 3, have been selected after a survey conducted among

Table 1
Heat sink manufacturing method's description, adapted from [37,45,46].

Process	Description	Materials
Extrusion	The metal is shaped by pushing it through an extrusion die.	Al
Die-casting	The molten metal is injected under high pressure into a mould.	Al, Zn-Alloy
Stamping	The metal is shaped by being pressed to a metal stamping die.	Al, Cu
Bonding	The fins are bonded to the base by thermal epoxy, brazing or soldering.	Al, Cu, Mg
Folding	A metal sheet is folded into a serpentine fin array and attached to the base by soldering or brazing.	Al, Cu
Forging	The material is forced into a moulding die by a punch.	Al, Cu
Skiving	Fins are sliced using a special machine and are bent at the base to form slender curved fins.	Al, Cu
Machining	Fins obtained by material removal, generally using a computer numerical control (CNC) machine.	Al, Cu, Mg

different suppliers and according to available references [7,41]. They have been kept constant, independent of the investigated cell dimensions.

3. Heat sink design

3.1. The heat sink temperature

Eq. (1) requires an input θ_b, which expresses the difference between the heat sink temperature (T_{HS}) and the ambient (T_{amb}). In accordance to the Concentrator Standard Operating Conditions (CSOC) [50] used in this work, a *DNI* of 900 W/m^2 and an ambient temperature of 20 °C have been considered. T_{HS} can then be calculated via the equation of the heat transfer in solids [51], by imposing a fixed temperature on the cell (T_{cell}). Considering the heat flux moving from the cell to the heat sink, the temperature of the heat sink (T_{HS}) can then be calculated as [7]:

$$T_{HS} = T_{cell} - Q_{cell} \cdot \frac{A}{k} \quad (6)$$

where T_{cell} is the cell temperature, Q_{cell} is the waste heat produced by the cell, the term A corresponds to the thermal exchanging surface area and k is the thermal conductivity of the material. This way, T_{HS} expresses the maximum heat sink temperature to keep the cell at T_{cell}. Two cell operating temperatures have been considered in the present work: 60 °C and 80 °C. These values fall within the optimal range of temperature recommended for HCPV cells [8,9]. Cell suppliers generally advise users to keep the cell at temperatures lower than 100 °C–120 °C [52–54]. However, a recent study has shown that keeping operating temperature higher than 80 °C can dramatically affect the durability of the cells, thereby deteriorating their reliability [55]. For this reason, the range of temperatures considered in this work has been limited to a maximum temperature of 80 °C under CSOC conditions.

The heat produced by the cell is mainly transferred by conduction to the heat sink [56], which then dissipates to the ambient by two mechanisms: radiation and convection [7]. Taking into account the following assumptions [16]:

- all the heat generated by the cell reaches the heat sink,
- both surfaces of the flat plate exchange heat with the ambient environment,
- a view factor of 1,
- an ambient temperature of 20 °C,

it is possible to calculate the minimum area (A_{HS}) a flat heat sink (without fins) would require to remove all the heat produced by the cell (Q_{cell}) under conditions of natural convection [16] as,

$$A_{HS} = \frac{Q_{cell}}{2 \cdot \left[h_c \cdot (T_{HS} - T_{amb}) + \sigma \cdot F_{i-k} \cdot \epsilon \cdot \left(T_{HS}^4 - T_{amb}^4\right)\right]} \quad (7)$$

where h_c is the heat transfer coefficient, which, at this stage, is set equal to 5 W/m^2 K [57]. The temperatures of the heat sinks for a 500× HCPV application, estimated with Eq. (6), are reported in Table 4, along with the parameters for a flat heat sink, calculated from Eq. (7). Considering the same cell temperature, the heat sinks made of Al and Cu achieve similar temperatures and require similar dimensions to handle the heat production. As shown in Table 4 though, despite the negligible difference in surface extension, the flat Cu heat sinks would weight much more than the Al ones, because of the strong difference in density between the materials. This difference is then enhanced when the cost is considered: it is almost one order of magnitude larger for copper, affected by both the highest density and the highest cost per unit of mass.

Table 2
Heat sink manufacturing methods, characteristics and costs adapted from [37,45–47]. The cost refers to a large-volume production (generally >5000 units per production run).

Process	Properties	Spacing ratio	Cost
Extrusion	• The most common process. • Low cost. • Low aspect ratios.	Low	$
Die-casting	• Rapid process. • Require high initial investments. • Lower thermal conductivity than extrusion.	Low	$
Stamping	• High volume manufacturing techniques. • Low performance heat sinks.	N.A.	$
Bonding	• Expensive manufacturing process. • Thermal and mechanical performance relies on the characteristics of the thermal paste.	High	$$$
Folding	• High flexibilities in the design of the heat sink. • Contact resistance due to soldering or brazing. • Lightweight. • Difficult to produce small pitches.	Medium/ High	$$$
Forging	• Production of high strength, rigid, uniform fin arrays.	High	$
Skiving	• Limited height and pitch for Cu. • Minimal tooling costs. • High fin density.	Medium	$$
Machining	• Fin arrays often damaged. • Large amount of material wasted.	High	$$

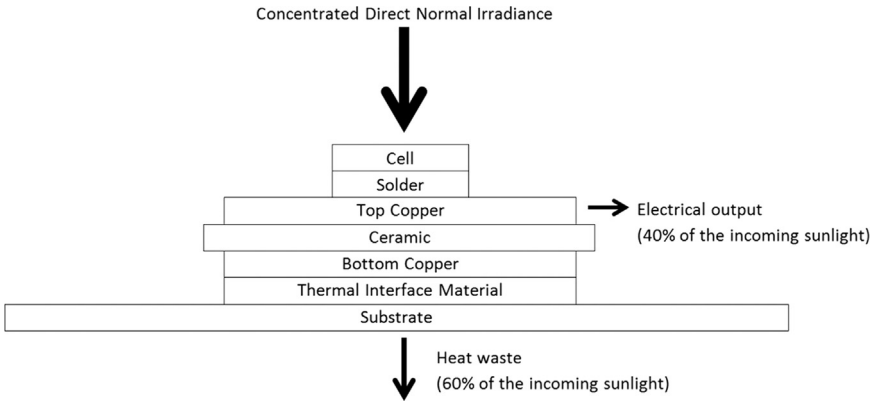

Fig. 2. Cross-section of a typical CPV receiver, together with energy flows. Relative dimensions are not to scale.

Fig. 3 shows the temperatures the heat sinks have to maintain in order to keep the HCPV cell at 80 °C for different concentrations. In accordance with the previous results, the temperature of aluminium is found to be lower. This is due to the lower thermal conductivity of aluminium compared to copper. Considering the same dimensions, the heat transferred by conduction (q_k) is proportional to the temperature difference and to the thermal conductivity of the material (k):

$$q_k = \frac{k}{l} \cdot A_k \cdot (T_{cell} - T_{HS}) \quad (8)$$

where A_k is the cross-section normal to the direction of the heat flux and l is the distance between the heat source and the heat sink. Therefore, in order to transfer the same amount of heat from the cell to the heat sink, the lower-conductive aluminium requires a bigger difference of temperature than the higher-conductive copper heat sink.

3.2. Flat heat sink

The most simple approach to handle the heat management of an HCPV system is a flat heat sink [15]. Ideally, in these cases, a surface as large as the concentrating optics is available for cooling. In order to analyse the thermal behaviour of a flat heat sink under different HCPV conditions, a thermal model has been developed using the "Heat transfer" module of COMSOL Multiphysics 4.4. The geometry of the receiver has been modelled as shown in Fig. 4.

Three proprieties for each material have been introduced as required by the software package (Table 5): the thermal conductivity, the density, and the heat capacity at constant pressure.

The solder paste and the thermal interface material have been reproduced as thin thermally resistive layers: for this function, COMSOL required as an input the thickness and the thermal conductivity only (Table 6).

The cell is set as a heat source, with a waste heat production equal to [58]:

$$Q_{cell} = C_{geo} \cdot DNI \cdot \eta_{opt} \cdot A_{cell} \cdot (1 - \eta_{cell}) \quad (9)$$

where C_{geo} is the geometric concentration of the system, n_{opt} is the optical efficiency of the concentrator and A_{cell} is the active area of the cell. Radiative and convective heat fluxes are applied to both the upward and downward surfaces of the receiver. The heat transfer coefficient is defined as follows [28]:

$$h_c = \frac{k}{L^*} \cdot 0.54 \cdot Ra_L^{0.25} \text{ for the upward facing surface} \left(\text{if } Ra_L \le 10^7\right) \quad (10)$$

$$h_c = \frac{k}{L^*} \cdot 0.15 \cdot Ra_L^{0.\overline{33}} \text{ for the upward facing surface} \left(\text{if } Ra_L > 10^7\right) \quad (11)$$

$$h_c = \frac{k}{L^*} \cdot 0.27 \cdot Ra_L^{0.25} \text{ for the downward facing surface} \quad (12)$$

where k is the thermal conductivity of the surface, L^* is the characteristic length, defined as the ratio between the area and the perimeter, and Ra_L is the Rayleigh number. It is expressed as:

$$Ra_L = \frac{g \cdot \beta \cdot L^{*3} \cdot (T_{HS} - T_{amb})}{\alpha \cdot \nu^*} \quad (13)$$

where g is the gravitational acceleration, β is the thermal expansion coefficient, α is the thermal diffusivity and ν is the mean kinematic viscosity of air. In addition, the same surface is set to exchange heat with the ambient by radiation as well. As shown in Fig. 5, COMSOL gives as an output the temperature distribution across the receiver, the maximum temperature shown in the figures is that achieved by the cell. A large temperature drop is developed between the cell and the heat sink; this is due to the low thermal conductivities of the cell and the solder layer, reported in Table 3. These layers act as thermal resistances that limit the heat flow from the cell to the heat sink and, therefore, increase the temperature difference between them.

The investigation has been conducted by taking into account different cell dimensions, different heat sink materials (Al or Cu) and different concentration factors. The maximum temperatures achieved by the cells have been recorded, and the results are resumed in Fig. 6. The cell temperature has a linear dependence on the concentration when a flat heat sink as large as the primary concentrator optics entrance aperture is used. The slope of the temperature characteristic varies with the cell sizes. The results show that the cooling of smaller cells can be easily handled by a flat heat sink. This means that the miniaturization of the cell is a positive initiative to consider in terms of HCPV cooling. By instead increasing the concentration and the cell size the thermal management is found to be more difficult and the temperature is found to increase. The use of a finned heat sink is expected to introduce a benefit to the system, with a reduction in cell temperature. The results show that aluminium heat sinks seem to be more affected by increased concentrations, when the largest cell is considered, as highlighted by the slope of the curve for a 10 mm cell in Fig. 6. By analysing the temperature gradient on the flat plate, shown in Fig. 7, it can be seen that the copper plate has a more uniform temperature distribution, due to the better thermal conductivity of copper compared to aluminium. This is because for large cells and high concentrations, the Cu plate provides better thermal management than one made of Al; the heat is more uniformly distributed across the surface of a copper plate than for an aluminium one. This advantage is minimised by the utilisation of smaller cells,

Table 3
Structure of the receiver, adapted from [7].

Layer	Material	Thickness [mm]	Thermal conductivity [W/m K]
Cell	Ge	0.18	60
Solder	SnAgCu	0.125	78
Top Copper	Cu	0.3	400
Ceramic	AlNi	0.63	285
Bottom Copper	Cu	0.3	400
Thermal interface material	Epo-tek	0.05	2.83
Substrate	Al or Cu	5	229 or 400 (respectively)

Table 4
Temperature and dimension of the flat HCPV heat sink. Conditions: concentration of 500 ×, optical efficiency of 85%, cell efficiency of 40%, 3 mm × 3 mm cell, 900 W/m^2 input, 20 °C ambient temperature, and heat transfer coefficient of 5 W/m^2 K.

Substrate material	Cell temperature [°C]	Heat sink temperature [°C]	Dimension of the flat heat sink [cm^2]	Ratio of heat sink area to cell area	Weight of the flat heat sink [kg]	Cost of the flat heat sink [USD]
Al	80	69	19	210	0.03	0.04
	60	49	34	374	0.05	0.07
Cu	80	71	19	208	0.08	0.38
	60	51	32	360	0.14	0.65

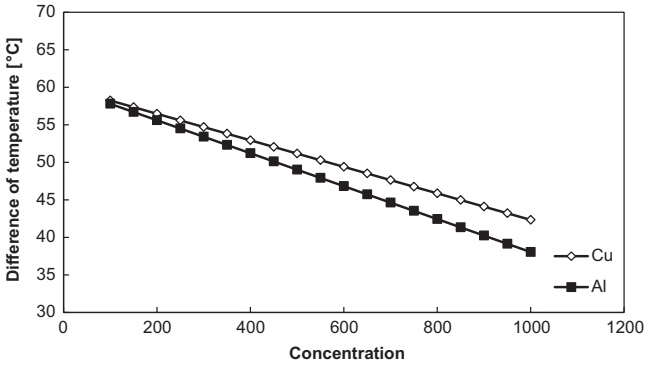

Fig. 3. Temperature difference between the flat heat sink and the ambient temperature depending on the heat sink material required to keep the 3 mm × 3 mm cell at a constant temperature of 80 °C. Conditions: optical efficiency of 85%, cell efficiency of 40%, 3 mm × 3 mm cell, 900 W/m^2 input, 80 °C cell temperature, 20 °C ambient temperature, 5 W/m^2 K heat transfer coefficient and 5 mm-thick substrate.

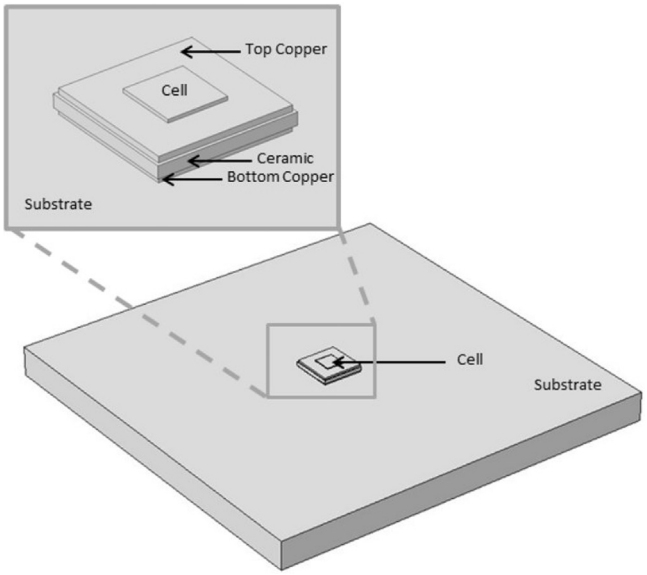

Fig. 4. Geometry of the receiver modelled in COMSOL for a 3 mm × 3 mm cell.

Table 5
Proprieties of materials used in the COMSOL simulation.

Materials	Thermal conductivity [W/K m]	Density [kg/m^3]	Heat Capacity [J/kg K]
Aluminium	160	2700	900
Aluminium Nitride	285	3260	740
Copper	400	8700	385
Germanium	60	5323	320

Table 6
Conductivity and thickness of the thermally resistive layers.

Materials	Thermal conductivity [W/K m]	Thickness [mm]
Solder paste	4.50	0.125
Thermal interface material	2.83	0.050

whose flat plate heat sinks have lower thermal gradients due to the smaller dimensions. So, within the considered range of concentrations, the heat sinks made of the two different materials are found to have similar thermal performance.

Any HCPV heat sink is expected to handle the thermal management of the cell even in case of the failure of the DC/AC inverter. Under these or analogous worst-case conditions, all the sunlight striking on the cell is converted into heat since the concentrator system is at open circuit. In these circumstances, the concentrator cells must withstand temperatures higher than those for normal operating conditions. The temperatures should be limited to avoid damage to the receiver's components. In order to widen the investigation on the reliability of flat plate heat sinks, the same COMSOL model has been used to predict the thermal behaviour of HCPV receivers under these worst-case conditions. Conditions of 900 W/m^2 *DNI*, 85% optical efficiency, no power output by the cell, and 20 °C ambient temperature have been considered. The results of a detailed analysis are summarised in Fig. 8 and confirm the previous findings: the two materials have similar heat dissipation abilities. Large cells under high concentrations reach dangerous temperatures, whereas the micro-cells show reasonable temperatures for open circuit and normal operating conditions, confirming that the miniaturization of the cells can lead to a simplification of the cooling systems. Depending on the cell size and the concentration, a rise in cell temperature between 10 and 40 °C occurs when the system goes from operating to worst case conditions.

In the present investigation, a fixed plate thickness of 5 mm has been considered. Thinner plates could have been selected and can be utilized for small cell dimensions, in order to reduce the cost and the weight of the HCPV system. On the other hand, thinner plates would have changed the resulting thermal performance. In this work, in order to get a better comparison among the thermal behaviours of analogous systems with different cell sizes, the thickness of the heat sinks have not been modified. In this way, the benefits that the miniaturization of the cells can provide to the thermal management of HCPV can be clearly shown. Similarly, different input values could have been considered. All the assumptions made in this work take into account a general HCPV system and are used to carry out a comparative study among different materials, cells sizes and concentrations. They can be changed in order to model any specific system or location.

The temperature of the cell relies not only on the concentration and on the cell size, but on many different factors, such as the irradiance or the ambient conditions [59]. The values reported in the figures take into account standard operating conditions, which could be different from the actual conditions [60]. For example, in case of higher ambient temperatures and lower efficiencies, the cell temperatures are expected to increase significantly. So, a flat surface might not be sufficient to keep the cell within the recommended range of 50–80 °C. In different circumstances, lower cell temperatures than those achieved by flat heat sink might be desirable. In these cases, the application of a finned heat sink can improve passive thermal management, even if the weight of the system is increased. In light of maximising the electrical performance of the HCPV system, it is important to understand the relationship between the cost and the performance of heat sink, as well as those between the design of the heat sink and the energy yield of HCPV systems, these aspects are investigated in the following sections.

3.3. Finned heat sink design

We explored the design of finned heat sinks using the LM approach. A concentration range between 100 and 1000 × has been considered, with a step of 50 × between each analysis. Each heat sink has been designed taking into account the heat generated by a 40% efficient multi-junction cell and the temperature differences obtained previously (Fig. 3). Copper and aluminium have been considered and two nominal cell temperatures of 60 °C and 80 °C have been modelled. Fig. 9 shows the volume of the finned

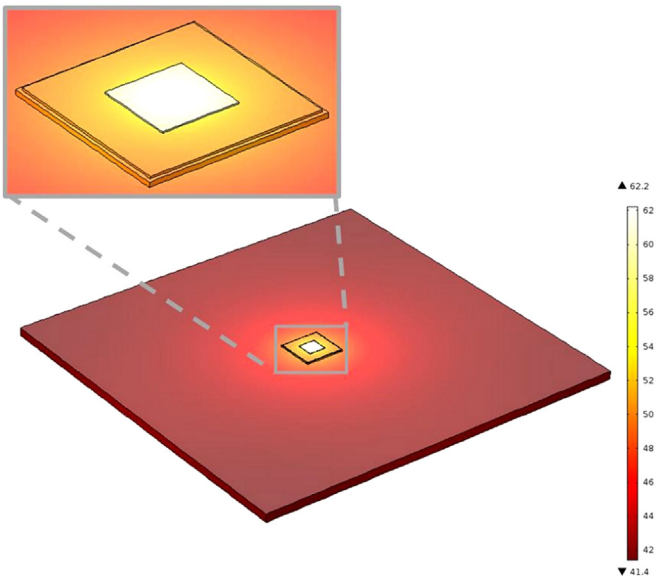

Fig. 5. Temperature distribution (in °C) across the cell assembly and a zoom in to the cell. Cell size is 10 mm × 10 mm. Concentration is 500 × . Conditions: 900 W/m^2 *DNI*, optical efficiency of 85%, cell efficiency of 40%, 20 °C ambient temperature. A 5 mm-thick aluminium substrate is considered. Cell temperature is 62.2 °C. Temperature of the top surface of aluminium substrate ranges between 50.7 °C and 41.4 °C.

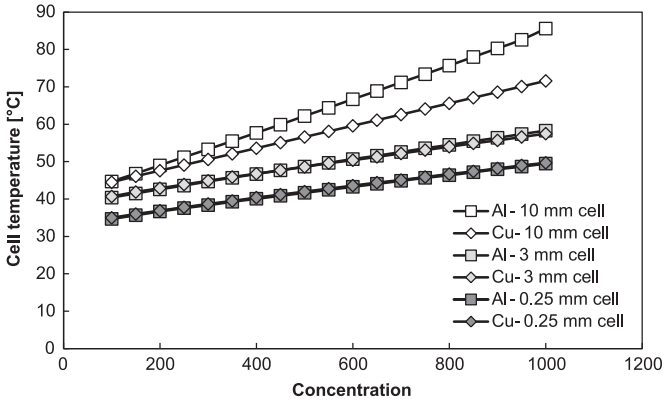

Fig. 6. Cell temperatures for different substrates and cell dimensions, depending on the geometric concentration. Conditions: 900 W/m^2 *DNI*, optical efficiency of 85%, cell efficiency of 40%, 20 °C ambient temperature, and 5 mm-thick substrate.

aluminium or copper heat sinks developed either to keep the cell at 60 °C or 80 °C. It is found that, under the same concentration value, LM heat sinks made of copper require slightly smaller volumes than LM heat sinks made of aluminium.

It is clear to see that the dependence versus volume is not always smooth when the concentration ratio increases. This is due to the fact that the LM approach has been developed to optimise the performance of the convective heat transfer, neglecting the contribution of radiation. In the present investigation, instead, the combined convective and radiative transfers are modelled. The view factors used to calculate the radiative heat transfer are strongly dependent on the geometry of the fins [35]. The most dramatic changes in the increase of volume take place when the number of fins increases, as highlighted in Fig. 10. An improvement in the model would bring to an optimisation of the combined contribution of energy dissipated by radiation and convection, and would thus lead to smoother behaviour. Although recommended, this initiative is beyond the scope of this work.

It is interesting to highlight that, taking into account the weight instead of the volume (Fig. 11), the difference between the two

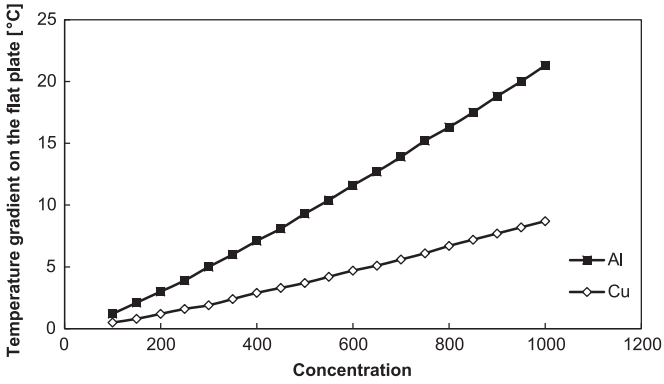

Fig. 7. Temperature gradient on the flat plate heat sink when a 10 mm × 10 mm-sized cell is exposed to different concentrations. Conditions: 900 W/m^2 *DNI*, optical efficiency of 85%, cell efficiency of 40%, 20 °C ambient temperature, and 5 mm-thick substrate.

materials is more pronounced, driven by the lower density of the aluminium. Aluminium heat sinks are found to have consistently lower weight than the copper ones. The best performance in terms of weight makes aluminium the best candidate for the manufacturing of heat sinks for cooling of HCPV cells, where the weight has a strong effect on the electrical performance of the system and, as we shall see, its cost per unit of energy production.

4. Cost analysis

Designers have to take into account two main parameters when designing the heat sink for an HCPV system: the cost and the effects on the system performance. The ideal goal is minimizing the costs and, at the same time, maximizing the system performance. In light of this, in the present section, the costs of the LM heat sinks are discussed. It was considered that the heat sinks were fabricated using the same processes as in the previous sections. Therefore, when comparing the costs of different heat sinks, the tooling, installation and manufacturing costs have not been considered. Only the material costs were accounted for, as reported in Section 2.3.

4.1. Costs vs. materials

The costs of the heat sinks previously presented are reported in Fig. 12. As expected, the aluminium heat sinks have been found to be less expensive than the copper ones, despite the lower thermal conductivity, because of the lower cost of the material, the lower volumes and the thermal performance compared to those of the copper heat sinks. These results support the use of aluminium heat sinks for HCPV applications.

Machining is one of the processes that allow the production of both copper and aluminium heat sinks. In this process fins are obtained by removing the excess materials. So, initially, a block of material as large as the heat sink base plate and as high as the whole heat sink has to be used. Therefore, the cost of the material is not directly related to the volume of the heat sink, but depends on the height and the length of the fins. The cost of the machined heat sink (c_{macHS}) can be calculated as:

$$c_{macHS} = \left[L \cdot W \cdot (H + tb)\right] \cdot \rho \cdot c_m \tag{14}$$

where ρ is the density of the material and c_m is the cost per unit of mass. Fig. 13 shows the difference in price between extruded and machined heat sinks made of aluminium. As expected, the machined heat sinks prices are higher than those found previously (see Fig. 12). A drop between 30% and 40% in cost is found when

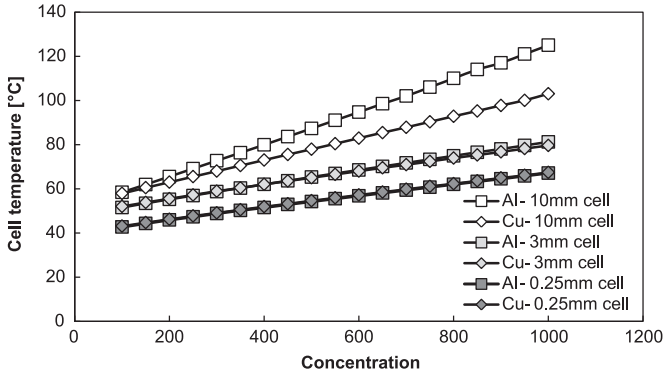

Fig. 8. Cell temperature for different substrates and cell dimensions versus the geometric concentration under the worst-case conditions. Conditions: 900 W/m^2 *DNI*, optical efficiency of 85%, open circuit (no power output), 20 °C ambient temperature, 5 mm-thick substrate. This figure can be compared with Fig. 6, which reports the data for the case of full power extraction.

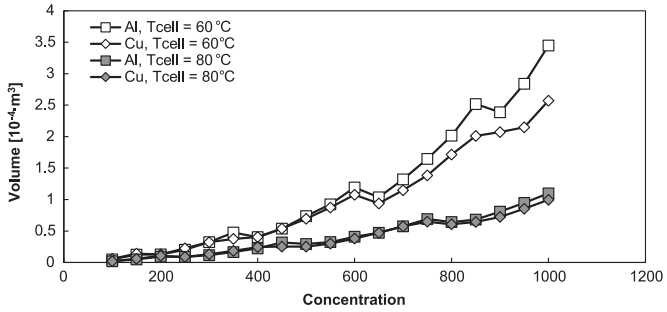

Fig. 9. The volume of the finned Least-Material heat sinks depending on the concentration. Cell size: 3 mm × 3 mm. Conditions: 900 W/m^2 *DNI*, optical efficiency of 85%, cell efficiency of 40%, and 20 °C ambient temperature.

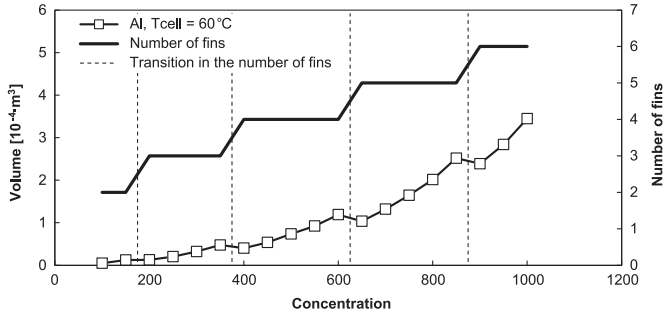

Fig. 10. The effect of a change in the number of fins on the volume of an aluminium LM heat sink, for a cell size of 3 mm × 3 mm. Conditions: 900 W/m^2 *DNI*, optical efficiency of 85%, cell efficiency of 40%, 20 °C ambient temperature. The vertical dotted lines mark the transitions between geometries with a different number of fins.

extrusion is employed compared to machining. Heat sink machining is subject to a waste of the excess material, which can be avoided by using other techniques shown in Table 1 and Table 2. For this reason, the use of extruded fins is generally preferred for mass production. This analysis did not take into account the fabrication costs, which are strongly influenced by the volume of heat sink produced, due to the high investment costs (e.g., in capital equipment) required by extrusion.

4.2. Costs vs. cell size

In order to analyse the effects of the cell size on the costs of the heat sink, only extruded aluminium fins have been further considered, due to the findings in the previous section that they should be preferred compared to those of copper. The results reported in the following figures have been obtained using the same methodology described before. As previously shown in Fig. 6, a cell size of 0.25 mm × 0.25 mm does not need a finned heat sink to be cooled to reasonable temperatures, and therefore has not been considered in the present investigation.

Fig. 14 shows the difference in costs for an extruded aluminium heat sink for two different sized cells at two temperatures. The costs of the heat sinks range between $0.03 and 0.9 per W_p depending on the cell size and the concentration. It is apparent that using smaller cells gives a strong benefit in terms of heat sink's mass and cost reductions. This result is confirmed in Fig. 15, where the costs per unit of installed peak power are reported. It is clearly shown that the cost per W_p of the heat sink increases with concentration ratio and cell size. Reducing the cell size from 10 mm to 3 mm can lead to a drop in price per unit of power up to 40% at high concentrations. In light of this, the development of new ultra-high concentration systems [61,62] strengthens the necessity of reducing the cell size in order to minimise the difficulties in the thermal management of the cells utilized. The miniaturization of the cell becomes particularly important when the CPV cost competiveness is taken into account. Indeed, as shown in Fig. 15, reducing the cost of the heat sink is an essential action to meet the cost per unit of power targeted by Ref. [63] and Ref. [3], for 2020 and 2030 respectively.

Horowitz et al. [22] considered a 25 mm^2 sized cell in a 30% efficient module under a 1000 × concentration and an optical efficiency between 0.80 and 0.85. The authors reported that, a passive aluminium heat sink would cost $0.6–0.7 per W_p. By taking into account the same conditions (1000 W/m^2 *DNI* and an aluminium cost of $2.2/kg), it has been found that the LM heat sink would cost between $0.5 and 0.8 per W_p depending on the cell temperature.

4.3. Heat sink costs vs. energy yield

In the previous sections, two cell working temperatures have been considered, 60 °C and 80 °C. Under real conditions, the lower cell operating temperature leads to a better energetic performance. However, this reduction in temperature has to be carefully planned to limit the costs of the heat sinks. For this reason, the energy yield for the four scenarios considered in Table 7 for two cells with different dimensions has been investigated. These scenarios (A–D) take into account two concentrations: 500 × and 1000 ×, and two nominal cell temperatures, 60 °C and 80 °C. The nominal temperature is the temperature that the cell would achieve under the reference conditions (*DNI* of 900 W/m^2, optical efficiency of 85%, cell efficiency of 40%, and air temperature of 20 °C). This temperature has been used to calculate the thermal resistance, as well of the cost of the aluminium heat sink in each scenario for the two cell sizes also shown in Table 7.

The energy harvested for the four scenarios and the two cell sizes is estimated for the following three worldwide locations:

- Solar Village (Saudi Arabia): lat. N 24° 54′25″, long. E 46° 23′49″
- Frenchman Flat (USA): lat. N 36° 48″32″, long. W 115° 56′06″
- Granada (Spain): lat. N 37° 09′50″, long. W 03° 36′18″.

Table 8 lists the annual average values of the main weather variables involved in the estimation of the energy yield at each location in order to show their climate characteristics.

The modelling techniques used to estimate the energy yield have been taken from the procedures previously discussed and experimentally validated in the literature [6,64]. The method described below, based on Eq. (15), has shown a root mean square error (RMSE) of around 3.5% and a mean bias error (MBE) of around −1.3% between actual and predicted data. The electrical power

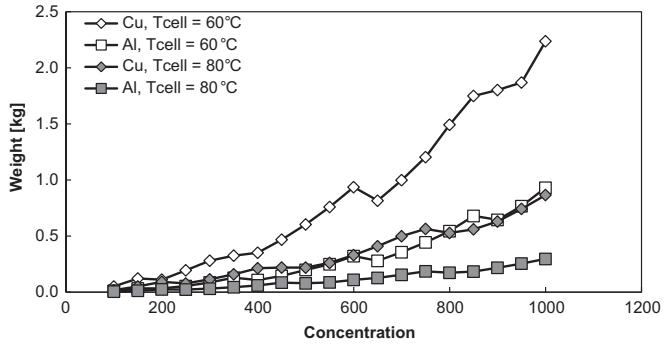

Fig. 11. The weight of the finned Least-Material heat sinks versus the geometric concentration. Conditions: 900 W/m^2 *DNI*, optical efficiency of 85%, cell efficiency of 40%, and 20 °C ambient temperature and cell size of 3 mm × 3 mm.

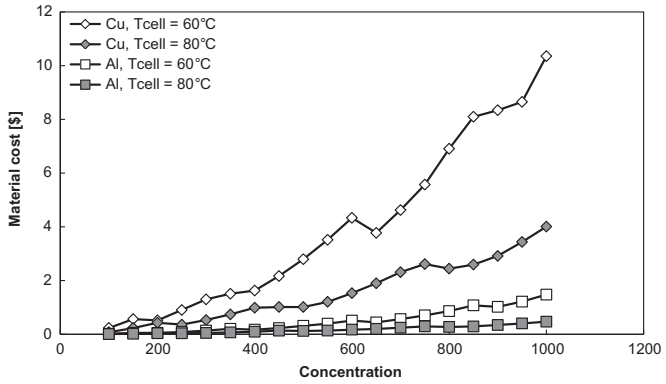

Fig. 12. The price of finned Least-Material heat sinks material versus the geometric concentration. Conditions: 900 W/m^2 *DNI*, optical efficiency of 85%, cell efficiency of 40%, 20 °C ambient temperature, and cell size of 3 mm × 3 mm.

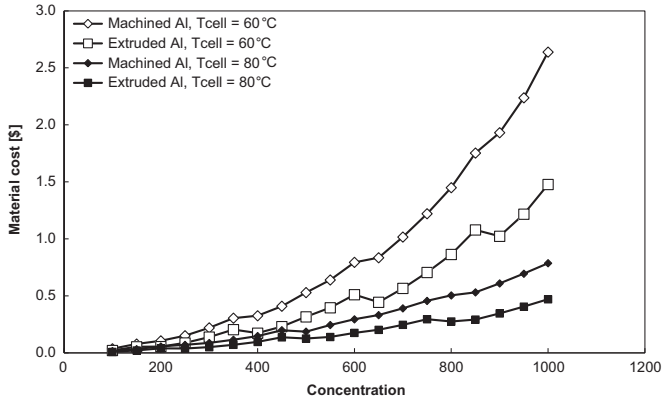

Fig. 13. Cost comparison of Al machining and extrusion. Cell size is 3 mm × 3 mm. Conditions: 900 W/m^2 *DNI*, optical efficiency of 85%, cell efficiency of 40%, and 20 °C ambient temperature.

output of the MJ solar cell under optical concentrated sunlight has been estimated as:

$$P_{cell} = DNI \cdot A_{cell} \cdot \eta_{opt} \cdot C_{geo} \cdot \eta_{cell} \cdot TF \cdot SF \quad (15)$$

where *DNI* is the input direct normal irradiance, A_{cell} the cell area, η_{opt} the optical efficiency, C_{geo} the geometric concentration of the system ($X = \eta_{opt} \cdot C_{geo}$), η_{cell} the efficiency of the cell at the operating concentration, *TF* the thermal factor and *SF* the spectral factor. *TF* quantifies the effect of the cell operating temperature on power as [9,65]:

$$TF = 1 - \gamma (T_{cell} - T^*_{cell}) \quad (16)$$

where γ is the maximum power temperature coefficient at the operating concentration (see Table 9 for the temperature coefficients), T_{cell} is the actual cell temperature and T_{cell}^* is the cell temperature under standard test conditions ($T_{cell}^* = 25$ °C). At the same time, the strong spectral dependence of HCPV devices has been estimated through SF as [66]:

$$SF = \frac{min\left(\int E_b(\lambda)\eta_{opt}(\lambda)SR_i(\lambda)d\lambda\right)\int E_{b,ref}(\lambda)d\lambda}{min\left(\int E_{b,ref}(\lambda)\eta_{opt}(\lambda)SR_i(\lambda)d\lambda\right)\int E_b(\lambda)d\lambda} \quad (17)$$

where the *i*-index represents the junction considered of the MJ solar cell, $E_b(\lambda)$ is the incident direct normal spectral distribution, $E_{b,ref}(\lambda)$ is the direct reference spectrum, $\eta_{opt}(\lambda)$ is the spectral optical efficiency of the concentrator and $SR(\lambda)$ is the spectral response of the *i*-junction of the MJ solar cell [6].

The amount and spectral distribution of the direct normal incidence (*DNI*) irradiance has been computed using the Simple Model of the Atmospheric Radiative Transfer of Sunshine (SMARTS) [68]. The air mass (AM) has been calculated as a function of the Sun's position [69], while the rest of the input parameters required by the SMARTS model (i.e. Aerosol optical depth at 550 nm, wavelength exponent and precipitable water) have been taken from the Aerosol Robotic Network (AERONET) data base [70]. The cell temperature has been calculated as [59,71]:

$$T_{cell} = T_{amb} + R \cdot Q_{cell} \quad (18)$$

where T_{amb} is the ambient temperature and *R* the thermal resistance (see Table 7 for the thermal resistances for each cell size and concentration ratio). The values of Q_{cell} are estimated from the values of *DNI* previously obtained using Eq. (9). The time series for the air temperature have been generated from the maximum, minimum and average values obtained from a NASA data source [72] using the Erbs model [73,74]. Finally, the maximum power has been estimated every ten minutes for the whole year as a function of the simulated values of *DNI*, *TF* and *SF*. Thus, the annual energy harvested can be estimated as:

$$E = \int P_{cell}(DNI, TF, SF)dt \quad (19)$$

Fig. 16 shows an example of the evolution of the simulated input parameters used to estimate the energy yield for a summer day at the Granada site. A similar behaviour is found during the whole year for the three locations under study. The *DNI* is minimum at sunrise and sunset, and maximum at midday. On the other hand, the spectral losses are minimum at midday, and maximum at sunrise and sunset. Regarding the cell temperature losses, they are maximum at midday, and minimum at sunrise and sunset. This behaviour is dominated by the daily profile of *DNI*. It is important to remark that the difference in the impact of cell temperature between the systems designed for a nominal cell temperature of 80 °C and the systems designed for 60 °C changes during the course of the day. Moreover, this difference tends to grow with the increase in *DNI*. This can be explained by considering the dependence of the cell operating temperature of the systems with the irradiance, as given in Eq. (18), and their different thermal resistances, as given in Table 7.

The results obtained for the four scenarios considered are presented in Fig. 17. As expected, the systems designed for a nominal cell temperature of 60 °C have a higher energy yield than the systems designed for 80 °C. This increase ranges from 1.8% (Granada) to 2.2% (Solar Village) for the concentration of 500 ×, and from 1.6% (Granada) to 1.9% (Solar Village) for the concentration of 1000 ×. The slightly lower enhancement with increasing concentration is produced by the reduction of the temperature coefficient (see Table 9) of maximum power as a function of concentration. This effect is also observed when comparing the impact

of cell temperature on the power output between the systems operating under 500 × and 1000 × shown at the bottom of Fig. 16.

It is worth mentioning that the procedure above estimates the DC energy of a concentrator from the properties of the MJ solar cells and optical devices used. The DC and AC energy yield of a whole HCPV system (i.e. modules, tracker, inverter and other balance of system components) can also be calculated from the rated power of the modules and by considering the electrical configuration of the system, as discussed in the literature [74]. This would allow the extension of the analysis performed in this section, in terms of the energy yield of a complete HCPV system, to be carried out.

The cost of cooling for the four scenarios and two cell areas has been estimated from the predicted values of energy yield and are plotted in Fig. 18 and Fig. 19 from:

$$\text{cost of cooling } (\$/\text{kWh}) = \frac{\text{cost of heat sink}(\$/Wp)}{\text{N} \cdot \text{annual energy yield}(kWh/Wp)} \quad (20)$$

where N is the useful life of the HCPV system, its value taken as 30 years in this analysis as previously discussed [23]. As can be seen, the cost of the cooling increases with concentration ratio and cell sizes. This is consistent with the results previously found and plotted in Fig. 15. Fig. 20 shows the relationship between the cost of the cooling for the system designed for 80 °C and 60 °C. An LM heat sink designed for a nominal cell temperature of 80 °C has a material cost per unit of energy generated by the system which is between 50% and 70% less expensive than that required by an LM heat sink designed for 60 °C (Fig. 20). These percentages are enhanced at higher concentrations, where they are limited by the size of the cell. This enhancement is the result of the higher cost of the heat sink per unit power versus concentration (see Fig. 15), as well as the lower energy increase by reducing the cell operating temperature (as a function of concentration). The outcome of the research presented here would then suggest limiting the dimensions of the cooling system at high concentrations. Oversizing the heat sink would lead to a strong increase in installation costs. It is important to note that the increase in the cost of the heat sink per unit power for the system designed for 60 °C and 80 °C is significantly higher than the error of the procedure used to estimate the energy yield of the systems. Hence, the impact of the uncertainty of the method described above for the prediction of the

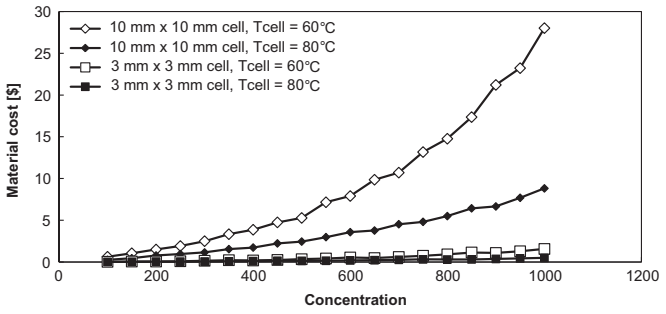

Fig. 14. Material costs for extruded Aluminium heat sinks versus geometric concentration. Conditions: 900 W/m^2 *DNI*, optical efficiency of 85%, cell efficiency of 40%, and 20 °C ambient temperature.

Table 7
The four scenarios considered in the energy yield and economical investigation.

Scenario	Concentration	Nominal cell temperature (°C)	Thermal resistance (K/W)		Cost of the LM aluminium heat sink ($/W$_p$)	
			10 mm	3 mm	10 mm	3 mm
A	500 ×	60	1.74	19.37	0.33	0.23
B		80	2.61	29.05	0.15	0.09
C	1000 ×	60	0.87	9.68	0.87	0.54
D		80	1.31	14.52	0.27	0.17

Table 8
Annual average values of the main atmospheric parameters for each site considered. Note that the mean values of the variables are averaged over the course of the day and then over the year, and that only values with *DNI* higher than 10 W/m^2 have been taken into account.

Location	*DNI* (W/m^2)	T_{amb} (°C)	AM
Solar village	694	28.8	3.0
Frenchman flat	704	18.4	3.3
Granada	623	19.1	3.3

Table 9
Temperature coefficients (γ) of the maximum power for the two concentrations levels investigated [67].

Concentration	Temperature coefficient of maximum power (%/K)
500	−0.13
1000	−0.11

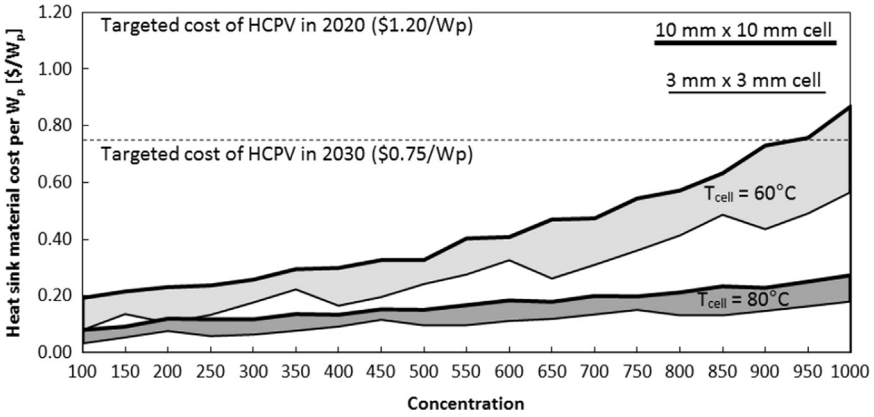

Fig. 15. Material costs per unit of installed power for extruded aluminium heat sinks versus geometric concentration. Conditions: 900 W/m^2 *DNI*, optical efficiency of 85%, cell efficiency of 40%, and 20 °C ambient temperature. The targeted costs of HCPV are sourced from Refs. [3,63]. The thicker lines represent the cost of LM heat sinks for 10 mm × 10 mm cells at 60 °C (light grey area) and 80 °C (dark grey area). Similarly, the thinner lines represent the cost of LM heat sinks for 3 mm × 3 mm cells at 60 °C (light grey area) and 80 °C (dark grey area).

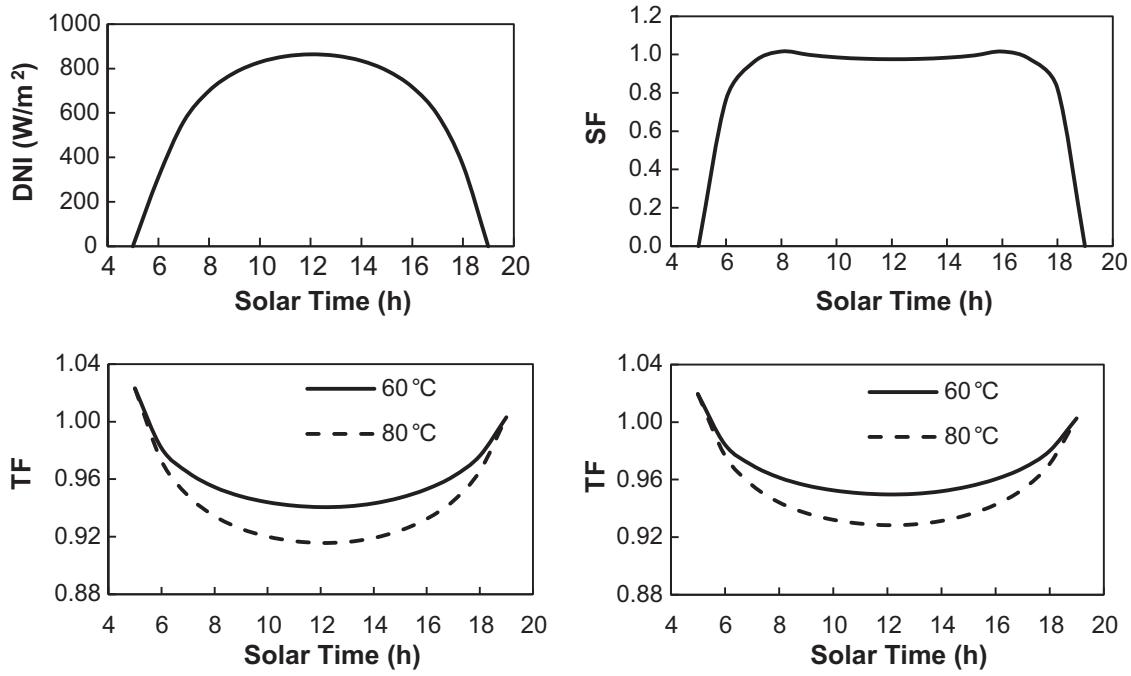

Fig. 16. Instantaneous value of *DNI* (top-left), impact of spectrum (top-right) and impact of cell temperature for 500 × (bottom-left) and 1000 × (bottom-right) for the two nominal cell temperatures considered vs. solar time for an example summer day, 15th of July, at Granada. The impact of cell temperature is independent of the area of the cell.

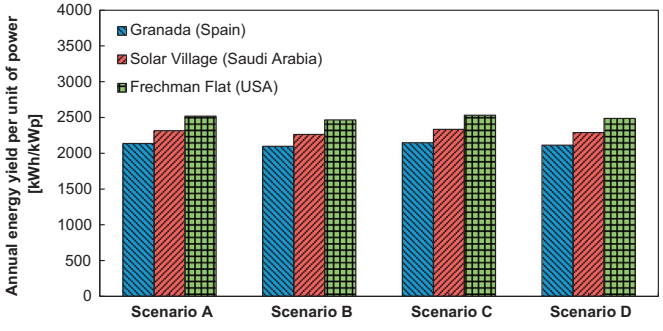

Fig. 17. Annual energy yield per unit of power by the HCPV systems for the three locations considered. Note that the annual energy yield is independent of the area of the cell, since the energy is given per unit of power of the concentrator (kWh/kW$_p$). Scenarios are described in Table 7. Extruded aluminium LM heat sinks have been considered.

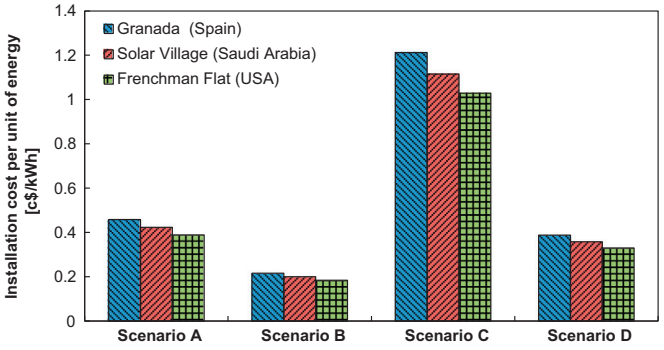

Fig. 18. Cost of the extruded aluminium LM heat sink per unit of energy produced by the HCPV system in 30 years by a 10 mm × 10 mm cell. The cooling cost per unit of energy is reported in USD cents per kWh (c$/kWh). The scenarios are described in Table 7.

annual energy harvested is not expected to have a relevant impact on the results found in this study.

The present work only took into account the material cost of the heat sinks, because the capital costs required by the fabrication are strictly related to the number of heat sinks. Therefore, the cost of the heat sink varies from case to case, depending on the geometry, the number of items produced and the materials. Designers can perform similar analysis to identify the optimal cooling system for each HCPV application and production volume. The aim of the present research is to contribute to the design of appropriate cooling systems and to determine limits and costs of passive cooling for HCPV applications. Further studies are recommended, to understand the effects of the heat sink size and performance on the levelised cost of electricity (LCOE) and to extend the range of materials, cell sizes and concentration studied in this investigation.

5. Conclusions

The main aim of the present work has been to investigate performance and costs for a passively cooled, single cell HCPV receiver whose concentration range is between 100 and 1000 × . In this light, optimized air-cooled heat sinks have been modelled and investigated. It has been found that aluminium performs better than copper as a heat sink material in terms of weight and costs. Despite the slightly higher volumes, under the same concentration and for the same conditions, the heat sinks made of aluminium would have lower weights and result in lower costs than those made of copper. This result is justified by the higher density and cost per unit of mass of copper compared to aluminium and to the similar thermal performance possessed by the two materials. In the present work, optimized finned heat sinks made of aluminium have shown the ability to keep a 3 mm × 3 mm cell temperature below 60 °C and 80 °C degrees under standard conditions at 1000 × with material costs of 0.57 \$/W$_p$ and 0.18 \$/W$_p$, respectively. Moreover, the reduction in size of the cells leads to a better thermal management of the systems. It has been found that a flat heat sink would be sufficient to cool a 0.25 mm-sided cell under high concentrations levels. So, the miniaturization of the cell, currently pursued by the academic community and industry, is

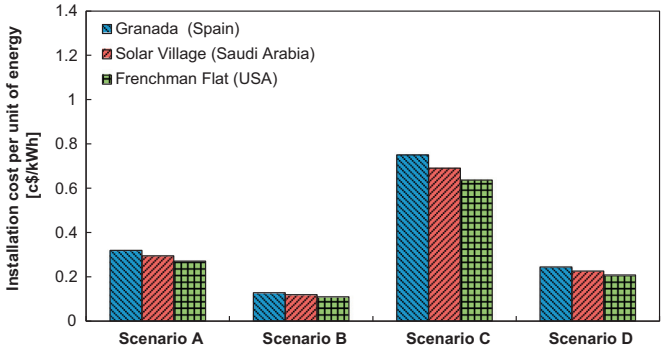

Fig. 19. Cost of the extruded aluminium LM heat sink per unit of energy produced by the HCPV system in 30 years by a 3 mm × 3 mm cell. The cooling cost per unit of energy is reported in USD cents per kWh (c$/kWh). The scenarios are described in Table 7.

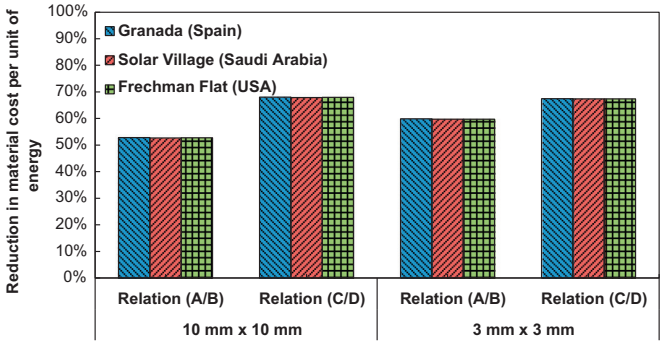

Fig. 20. Reduction in the cost of the extruded aluminium LM heat sink material per unit of energy produced between systems designed for 80 °C and 60 °C. Relation (A/B) expresses the reduction in cost per unit of energy obtained when a heat sink for a 500 × HCPV system is designed for 80 °C, instead of 60 °C. Similarly, Relation (C/D) expresses the reduction in cost per unit of energy obtained when a heat sink for a 1000 × HCPV system is designed for 80 °C, instead of 60 °C.

strongly recommended, especially, given the interest in ultra-high concentrator systems. Additionally, increasing concentration values have been found to increase the heat sinks cost per unit of power installed and energy produced. The cost of a heat sink able to cool a 3 mm × 3 mm cell at 1000 × is almost double than that used at 500 × . The energy yield of HCPV systems cooled using passive heat sinks with flat and finned geometries and made of Cu or Al materials has provided useful insights. Due to the small temperature coefficients of multijunction cells, the increase in the cost per unit of energy of a better-performing heat sink can be larger than the improvement in energy production obtained (compared to a lower-performing heat sink). This means that developing oversized heat sinks would lead to a percentage increase in cost higher than that in energy production, and that smaller heat sinks should be generally preferred.

In the present work, a simple rectangular plate-fin geometry has been considered. Many different geometries have been proposed and explored experimentally and should be investigated in future work in order to explore further increases in the thermal performance of the heat sinks per unit of mass. Despite the better performance offered by aluminium, it is important to remark that copper has a higher thermal conductivity than aluminium and, for this reason, it can spread heat across the heat sink in a more uniform way. The LM approach does not take into account the distribution of heat across the fin base, which becomes particularly important in practical implementations of HCPV, where the generation of heat is concentrated on a surface much smaller than the heat sink. This phenomenon should be considered in future work.

Acknowledgements

This work has been carried out within the EPSRC-funded BioCPV project (EP/J000345/1), duly acknowledged. Eduardo F. Fernández is supported by the Spanish Economy Ministry and the European Regional Development Fund/Fondo Europeo de Desarrollo Regional (ERDF/FEDER) under the project ENE2013-45242-R and the Juan de la Cierva 2013 fellowship.

References

[1] S. Kurtz, Opportunities and challenges for development of a mature concentrating photovoltaic power industry, Golden, CO, 2011. ⟨http://www.nrel.gov/docs/fy13osti/43208.pdf⟩ (accessed 19.4.16).
[2] P. Pérez-Higueras, E. Muñoz, G. Almonacid, P.G. Vidal, High concentrator photovoltaics efficiencies: present status and forecast, Renew. Sustain. Energy Rev. 15 (2011) 1810–1815, http://dx.doi.org/10.1016/j.rser.2010.11.046.
[3] S.P. Philipps, A.W. Bett, K. Horowitz, S. Kurtz, Current status of concentrator photovoltaic (CPV) technology, 2015. ⟨https://www.ise.fraunhofer.de/en/publications/veroeffentlichungen-pdf-dateien-en/studien-und-konzeptpapiere/current-status-of-concentrator-photovoltaic-cpv-technology.pdf⟩ (accessed 19.4.16).
[4] M.A. Green, K. Emery, Y. Hishikawa, W. Warta, E.D. Dunlop, Solar cell efficiency tables (version 47), Prog. Photovolt. Res. Appl. 24 (2016) 3–11, http://dx.doi.org/10.1002/pip.2728.
[5] A. Luque, S. Hegedus, Handbook of Photovoltaic Science and Engineering, John Wiley & Sons, Ltd, Chichester, UK (2003) http://dx.doi.org/10.1002/0470014008.
[6] E.F. Fernández, A.J.G. Loureiro, G.P. Smestad, Multijunction Concentrator Solar Cells: Analysis and Fundamentals, in: P. Pérez-Higueras, E.F. Fernández (Eds.), High concentrator photovoltaics fundamentals, engineering and power plants, Springer International Publishing, http://dx.doi.org/10.1007/978-3-319-15039-0.
[7] P. Rodrigo, L. Micheli, F. Almonacid, The High-Concentrator Photovoltaic Module, in: P. Pérez-Higueras, E.F. Fernández (Eds.), High concentrator photovoltaics fundamentals, engineering and power plants, Springer International Publishing, 2015, pp. 115–151, http://dx.doi.org/10.1007/978-3-319-15039-0_5.
[8] G.S. Kinsey, K.M. Edmondson, Spectral response and energy output of concentrator multijunction solar cells, Prog. Photovolt. Res. Appl. 17 (2009) 279–288, http://dx.doi.org/10.1002/pip.875.
[9] E.F. Fernández, F. Almonacid, P. Rodrigo, P. Pérez-Higueras, Calculation of the cell temperature of a high concentrator photovoltaic (HCPV) module: a study and comparison of different methods, Sol. Energy Mater. Sol. Cells 121 (2014) 144–151, http://dx.doi.org/10.1016/j.solmat.2013.11.009.
[10] G. Martinelli, M. Stefancich, 7 Solar Cell Cooling, in: A.L. Luque, A. Viacheslav (Eds.), Concentrator photovoltaics, Springer, Berlin, Germany, 2007, pp. 133–149.
[11] L. Micheli, N. Sarmah, X. Luo, K.S. Reddy, T.K. Mallick, Opportunities and challenges in micro- and nano-technologies for concentrating photovoltaic cooling: a review, Renew. Sustain. Energy Rev. 20 (2013) 595–610, http://dx.doi.org/10.1016/j.rser.2012.11.051.
[12] S. Jakhar, M.S. Soni, N. Gakkhar, Historical and recent development of concentrating photovoltaic cooling technologies, Renew. Sustain. Energy Rev. 60 (2016) 41–59, http://dx.doi.org/10.1016/j.rser.2016.01.083.
[13] A. Royne, C.J. Dey, D.R. Mills, Cooling of photovoltaic cells under concentrated illumination: a critical review, Sol. Energy Mater. Sol. Cells 86 (2005) 451–483, http://dx.doi.org/10.1016/j.solmat.2004.09.003.
[14] F. Gualdi, O. Arenas, A. Vossier, A. Dollet, V. Aimez, R. Arès, Determining passive cooling limits in CPV using an analytical thermal model, AIP Conf. Proc. 1556 (2013) 10–13, http://dx.doi.org/10.1063/1.4822187.
[15] K. Araki, H. Uozumi, M. Yamaguchi, A simple passive cooling structure and its heat analysis for 500 × concentrator PV module, in: Proceedings of the Twenty-Ninth IEEE Photovoltaic Specialists Conference, 2002, (n.d.), pp. 1568–1571. doi: ⟨http://dx.doi.org/10.1109/PVSC.2002.1190913⟩.
[16] L. Micheli, S. Senthilarasu, K.S. Reddy, T.K. Mallick, Applicability of silicon microfinned heat sinks for 500 × concentrating photovoltaics systems, J. Mater. Sci. 50 (2015) 5378–5388, http://dx.doi.org/10.1007/s10853-015-9065-2.
[17] M. Theristis, T.S.O. Donovan, Electrical-thermal analysis of III–V triple-junction solar cells under variable spectra and ambient temperatures, Sol. Energy. 118 (2015) 533–546, http://dx.doi.org/10.1016/j.solener.2015.06.003.
[18] I. Luque-Heredia, J.M. Moreno, P.H. Magalhães, R. Cervantes, G. Quéméré, O. Laurent, Inspira's CPV Sun Tracking, in: A.L. Luque, A. Viacheslav (Eds.), Concentrator photovoltaics, Springer, Berlin, 2007, pp. 221–251, http://dx.doi.org/10.1007/978-3-540-68798-6_11.

[19] P. Pérez-Higueras, F.J. Muñoz-Rodríguez, C. Adame-Sánchez, L. Hontoria-García, C. Rus-Casas, A. González-Rodríguez, et al., High-Concentrator Photovoltaic Power Plants: Energy Balance and Case Studies, in: P. Pérez-Higueras, E. F. Fernández (Eds.), High concentrator photovoltaics. fundamentals, engineering and power plants, Springer, Cham, Switzerland, 2015, pp. 443–477, http://dx.doi.org/10.1007/978-3-319-15039-0_16.

[20] J. Leloux, E. Lorenzo, B. García-Domingo, J. Aguilera, C. a Gueymard, A bankable method of assessing the performance of a CPV plant, Appl. Energy 118 (2014) 1–11, http://dx.doi.org/10.1016/j.apenergy.2013.12.014.

[21] G. Timò, Results of the APOLLON project and concentrating photovoltaic perspective, 2014, p. 95. ⟨http://www.rse-web.it/applications/webwork/site_rse/local/doc-rse/Results of the Apollon Projects/index.html⟩ (accessed 19.4.16).

[22] K.A.W. Horowitz, M. Woodhouse, H. Lee, G.P. Smestad, A bottom-up cost analysis of a high concentration PV module, AIP Conf. Proc. 1679 (2016) 100001, http://dx.doi.org/10.1063/1.4931548.

[23] D.L. Talavera, P. Pérez-Higueras, J. a Ruíz-Arias, E.F. Fernández, Levelised cost of electricity in high concentrated photovoltaic grid connected systems: spatial analysis of Spain, Appl. Energy 151 (2015) 49–59, http://dx.doi.org/10.1016/j.apenergy.2015.04.072.

[24] E.F. Fernández, D.L. Talavera, F.M. Almonacid, G.P. Smestad, Investigating the impact of weather variables on the energy yield and cost of energy of grid-connected solar concentrator systems, Energy 106 (2016) 790–801, http://dx.doi.org/10.1016/j.energy.2016.03.060.

[25] C. Min, C. Nuofu, Y. Xiaoli, W. Yu, B. Yiming, Z. Xingwang, Thermal analysis and test for single concentrator solar cells, J. Semicond. 30 (2009) 044011, http://dx.doi.org/10.1088/1674-4926/30/4/044011.

[26] M. Renzi, L. Egidi, G. Comodi, Performance analysis of two 3.5k Wp CPV systems under real operating conditions, Appl. Energy 160 (2015) 687–696, http://dx.doi.org/10.1016/j.apenergy.2015.08.096.

[27] F. Gualdi, O. Arenas, A. Vossier, A. Dollet, V. Aimez, R. Arès, Determining passive cooling limits CPV using analytical thermal model, AIP Conf. Proc. 1556, 2013, 10,http://dx.doi.org/10.1063/1.4822187.

[28] F.P. Incropera, D.P. DeWitt, T.L. Bergman, A.S. Lavine, Fundamentals of Heat and Mass Transfer, Wiley, Hoboken, NJ, 2007.

[29] N. Nagarani, K. Mayilsamy, a Murugesan, G.S. Kumar, Review of utilization of extended surfaces in heat transfer problems, Renew. Sustain. Energy Rev. 29 (2014) 604–613, http://dx.doi.org/10.1016/j.rser.2013.08.068.

[30] S.K. Natarajan, T.K. Mallick, M. Katz, S. Weingaertner, Numerical investigations of solar cell temperature for photovoltaic concentrator system with and without passive cooling arrangements, Int. J. Therm. Sci. 50 (2011) 2514–2521, http://dx.doi.org/10.1016/j.ijthermalsci.2011.06.014.

[31] K.H. Do, T.H. Kim, Y.-S. Han, B.-I. Choi, M.-B. Kim, General correlation of a natural convective heat sink with plate-fins for high concentrating photovoltaic module cooling, Sol. Energy 86 (2012) 2725–2734, http://dx.doi.org/10.1016/j.solener.2012.06.010.

[32] L. Micheli, K.S. Reddy, T.K. Mallick, Plate micro-fins in natural convection: an opportunity for passive concentrating photovoltaic cooling, Energy Procedia 82 (2015) 301–308, http://dx.doi.org/10.1016/j.egypro.2015.12.037.

[33] International Electrotechnical Commission, Concentrator photovoltaic (CPV) modules and assemblies–design qualification and type approval, IEC 62108 Ed.1.0, 2007.

[34] A. Bar-Cohen, M. Iyengar, A.D. Kraus, Design of optimum plate-fin natural convective heat sinks, J. Electron. Packag. 125 (2003) 208, http://dx.doi.org/10.1115/1.1568361.

[35] N.V. Suryanarayana, Engineering Heat Transfer, West Publishing Company, Minneapolis/St. Paul, 1995.

[36] G. Mittelman, A. Dayan, K. Dado-Turjeman, A. Ullmann, Laminar free convection underneath a downward facing inclined hot fin array, Int. J. Heat Mass Transf. 50 (2007) 2582–2589, http://dx.doi.org/10.1016/j.ijheatmasstransfer.2006.11.033.

[37] Y. Shabany, Heat Transfer: Thermal Management of Electronics, CRC Press, Boca Raton, Florida, 2009.

[38] Y.K. Khor, Y.M. Hung, B.K. Lim, On the role of radiation view factor in thermal performance of straight-fin heat sinks, Int. Commun. Heat Mass Transf. 37 (2010) 1087–1095, http://dx.doi.org/10.1016/j.icheatmasstransfer.2010.06.012.

[39] D.P. Kulkarni, D.K. Das, Analytical and numerical studies on microscale heat sinks for electronic applications, Appl. Therm. Eng. 25 (2005) 2432–2449, http://dx.doi.org/10.1016/j.applthermaleng.2004.12.010.

[40] Y.N. Wang, T.T. Lin, J.C. Leong, Y.T. Hsu, C.P. Yeh, P.H. Lee, et al., Numerical investigation of high-concentration photovoltaic module heat dissipation, Renew. Energy 50 (2013) 20–26, http://dx.doi.org/10.1016/j.renene.2012.06.016.

[41] Mecc.Al srl, Profilmecc & ProfilmeccPlus folder, 2013. ⟨http://www.meccal.com/pannello/amministrazione/download/1379436994_meccal pieghevole profilmecc standard tutto.pdf⟩ (accessed 19.4.16).

[42] S. Mahmoud, R. Al-Dadah, D.K. Aspinwall, S.L. Soo, H. Hemida, Effect of micro fin geometry on natural convection heat transfer of horizontal microstructures, Appl. Therm. Eng. 31 (2011) 627–633, http://dx.doi.org/10.1016/j.applthermaleng.2010.09.017.

[43] London metal exchange, Average official and settlement prices US$/tonne for the month of December 2015. ⟨https://www.lme.com/~/media/Files/Market data/Historic Data/2015/December 2015.xlsx⟩ (accessed 19.4.16).

[44] Y.A. Çengel, Introduction to Thermodynamics and Heat Transfer, Second ed., McGraw-Hill, New York, NY, 2008.

[45] M. Iyengar, Design for manufacturability of forced convection air cooled fully ducted heat sinks, Electron. Cool. (2007) (accessed 19.4.16)⟨http://www.electronics-cooling.com/2007/08/design-for-manufacturability-of-forced-convection-air-cooled-fully-ducted-heat-sinks/⟩.

[46] I. Advanced thermal solutions, heat sink: manufactoring technologies, Qpedia, 2010, pp. 22–26. ⟨www.qats.com/Download/Qpedia_Nov10_HS_manuf_technologies1.ashx⟩ (accessed 19.4.16).

[47] S. Lee, Optimum design and selection of heat sinks, IEEE Trans. Compon. Packag. Manuf. Technol. Part A. 18 (1995) 812–817, http://dx.doi.org/10.1109/95.477468.

[48] G. Peharz, J.P. Ferrer Rodríguez, G. Siefer, A.W. Bett, A method for using CPV modules as temperature sensors and its application to rating procedures, Sol. Energy Mater. Sol. Cells 95 (2011) 2734–2744, http://dx.doi.org/10.1016/j.solmat.2011.03.030.

[49] T. Chou, Z. Shih, H. Hong, C. Han, K. Chiang, Thermal performance assessment and validation of high-concentration photovoltaic solar cell module, IEEE Trans. Compon. Packag. Manuf. Technol. 2 (2012) 578–586, http://dx.doi.org/10.1109/TCPMT.2011.2181165.

[50] IEC, IEC 62670-1 Concentrator photovoltaic (CPV) module and assembly performance testing and energy rating – part 1: performance measurements and power rating – irradiance and temperature, 2012.

[51] A.F.A. Mills, Basic Heat and Mass Transfer, 2nd ed., Prentice Hall, London, UK, 1999.

[52] AZURSPACE solar power GmbH, Concentrator triple junction solar cell–type 3C42 data sheet, 2014. ⟨http://www.azurspace.com/images/pdfs/DB_3879-00-00_3C42_AzurDesign_3x3_20140226.pdf⟩ (accessed 19.4.16).

[53] Spectrolab Inc., CPV point focus solar cells–type C3MJ+Data sheet, 2011. ⟨http://www.spectrolab.com/DataSheets/PV/CPV/C3MJ_PLUS_2011.pdf⟩ (accessed 19.4.16).

[54] G. Segev, G. Mittelman, A. Kribus, Equivalent circuit models for triple-junction concentrator solar cells, Sol. Energy Mater. Sol. Cells 98 (2012) 57–65, http://dx.doi.org/10.1016/j.solmat.2011.10.013.

[55] P. Espinet-González, C. Algora, N. Núñez, V. Orlando, M. Vázquez, J. Bautista, et al., Temperature accelerated life test on commercial concentrator III–V triple-junction solar cells and reliability analysis as a function of the operating temperature, Prog. Photovolt. Res. Appl. 23 (2015) 559–569, http://dx.doi.org/10.1002/pip.2461.

[56] H. Cotal, J. Frost, Heat transfer modeling of concentrator multijunction solar cell assemblies using finite difference techniques, in: Proceedings of the 35th IEEE Photovoltaic Specialists Conference (PVSC) 2010, pp. 000213–000218.

[57] I. Mudawar, Assessment of high-heat-flux thermal management schemes, IEEE Trans. Compon. Packag. Technol. 24 (2001) 122–141, http://dx.doi.org/10.1109/6144.926375.

[58] E.F. Fernández, P. Rodrigo, F. Almonacid, P. Pérez-Higueras, A method for estimating cell temperature at the maximum power point of a HCPV module under actual operating conditions, Sol. Energy Mater. Sol. Cells 124 (2014) 159–165, http://dx.doi.org/10.1016/j.solmat.2014.01.050.

[59] F. Almonacid, P.J. Pérez-Higueras, E.F. Fernández, P. Rodrigo, Relation between the cell temperature of a HCPV module and atmospheric parameters, Sol. Energy Mater. Sol. Cells 105 (2012) 322–327, http://dx.doi.org/10.1016/j.solmat.2012.06.043.

[60] M. Muller, S. Kurtz, M. Steiner, G. Siefer, Translating outdoor CPV I–V measurements to a CSTC power rating and the associated uncertainty, Prog. Photovolt. Res. Appl. (2015), http://dx.doi.org/10.1002/pip.2590.

[61] L. Micheli, E.F. Fernández, F. Almonacid, K.S. Reddy, T.K. Mallick, Enhancing ultra-high CPV passive cooling using least-material finned heat sinks, AIP Conf. Proc. 1679, 2016, 130003, http://dx.doi.org/10.1063/1.4931563.

[62] A. Vossier, D. Chemisana, G. Flamant, A. Dollet, Very high fluxes for concentrating photovoltaics: considerations from simple experiments and modeling, Renew. Energy 38 (2012) 31–39, http://dx.doi.org/10.1016/j.renene.2011.06.036.

[63] B. Prior, Roadmap for CPV technology: a study conducted by GTM research, 2011, pp. 1–8. ⟨http://www.solarnovus.com/pdfs/GTM_CPV_Consortium_presentation.pdf⟩ (accessed 19.4.16).

[64] E.F. Fernández, F. Almonacid, A. Soria-Moya, J. Terrados, Experimental analysis of the spectral factor for quantifying the spectral influence on concentrator photovoltaic systems under real operating conditions, Energy 90 (2015) 1878–1886, http://dx.doi.org/10.1016/j.energy.2015.07.015.

[65] G. Peharz, J.P. Ferrer Rodríguez, G. Siefer, A.W. Bett, Investigations on the temperature dependence of CPV modules equipped with triple-junction solar cells, Prog. Photovolt. Res. Appl. 19 (2011) 54–60, http://dx.doi.org/10.1002/pip.987.

[66] E.F. Fernández, F. Almonacid, J. a Ruiz-Arias, a Soria-Moya, Analysis of the spectral variations on the performance of high concentrator photovoltaic modules operating under different real climate conditions, Sol. Energy Mater. Sol. Cells 127 (2014) 179–187, http://dx.doi.org/10.1016/j.solmat.2014.04.026.

[67] E.F. Fernández, G. Siefer, M. Schachtner, A. J. García Loureiro, P. Pérez-Higueras, Temperature coefficients of monolithic III–V triple-junction solar cells under different spectra and irradiance levels, AIP Conf. Proc. 1477, 2012, 189, http://dx.doi.org/10.1063/1.4753865.

[68] C. Gueymard, Parameterized transmittance model for direct beam and circumsolar spectral irradiance, Sol. Energy 71 (2001) 325–346.

[69] F. Kasten, A.T. Young, Revised optical air mass tables and approximation formula, Appl. Opt. 28 (1989) 4735–4738, http://dx.doi.org/10.1364/AO.28.004735.
[70] NASA, aerosol robotic network [Online]: ⟨http://aeronet.gsfc.nasa.gov/⟩, 2015. ⟨http://aeronet.gsfc.nasa.gov/⟩ (accessed 19.4.16).
[71] E.F. Fernández, F. Almonacid, A new procedure for estimating the cell temperature of a high concentrator photovoltaic grid connected system based on atmospheric parameters, Energy Convers. Manag. 103 (2015) 1031–1039, http://dx.doi.org/10.1016/j.enconman.2015.07.034.
[72] NASA, surface meteorology and solar energy [Online]: ⟨https://eosweb.larc.nasa.gov/sse/⟩, 2015. ⟨https://eosweb.larc.nasa.gov/sse/⟩ (accessed 19.4.16).
[73] F. Almonacid, P. Pérez-Higueras, P. Rodrigo, L. Hontoria, Generation of ambient temperature hourly time series for some Spanish locations by artificial neural networks, Renew. Energy 51 (2013) 285–291, http://dx.doi.org/10.1016/j.renene.2012.09.022.
[74] E.F. Fernández, P. Pérez-Higueras, F. Almonacid, J.A. Ruiz-Arias, P. Rodrigo, J. I. Fernandez, et al., Model for estimating the energy yield of a high concentrator photovoltaic system, Energy 87 (2015) 77–85, http://dx.doi.org/10.1016/j.energy.2015.04.095.